Research Article

Dynamic Indentation Characteristics for Various Spacings and Indentation Depths: A Study Based on Laboratory and Numerical Tests

Jie Liu [ID],[1,2] Wen Wan,[1] Yu Chen [ID],[3,4] and Jun Wang[2]

[1]*School of Resource, Environment and Safety Engineering, Hunan University of Science and Technology,
 Xiangtan, Hunan, China*
[2]*Department of Building Engineering, Hunan Institute of Engineering, Xiangtan, China*
[3]*School of Resource and Safety Engineering, Central South University, Changsha, Hunan, China*
[4]*State Key Laboratory for Geomechanics and Deep Underground Engineering, Beijing 100083, China*

Correspondence should be addressed to Jie Liu; ljydslj1@163.com and Yu Chen; yu.c@outlook.com

Laboratory and numerical study tests were conducted to investigate the dynamic indentation characteristics for various spacings and indentation depths. First, laboratory tests indicate that the increase in the indentation depth first resulted in enlarged groove volumes, caused by fiercer rock breakages between indentations for a fixed spacing; then, the groove volume slightly increased for further increase in indentation depth, whereas the increase in spacing restrained rock breakages and resulted in shrunken grooves. In addition, the numerical study agreed well with laboratory tests that small chips formed at the shallow part of the rock specimen at the early indentation stage, and then, larger chips formed by the crack propagation at deeper parts of the rock specimens when the indentation depth increased. With further increase in indentation depth, crushed powders instead of chips formed. Moreover, the numerical analysis indicates that crack propagation usually leads to the decrease of the indentation force and the dissipation of the stress concentrations at crack tips, whereas the cessation of crack propagation frequently resulted in the increase of the indentation force and the stress concentrations at crack tip with the increase in indentation depth.

1. Introduction

Indentations by excavation tools have been widely used to simulate the rock breakage process that determines the indentation efficiency. Extensive field, laboratory, and numerical studies indicated that cutting efficiency is affected by many factors, including geological and machinery factors. For the effect of geological factors (joint distributions, confining stresses, and rock property) on cutting efficiency, first, intermittent discontinuities widely distribute in rock masses, thus, previous studies proposed that these discontinuities in rock specimens significantly affect the indentation efficiency because these discontinuities affect the coalescence of the cracks in the rock [1–3]. Gong et al. indicated that joint spacing significantly affects the rock

breakage mode and further influences the cutting efficiency [4]. In addition, the laboratory tests by Yin et al. and Liu et al. denoted that confinements significantly affect crack propagation by indentations, and then further affect the indentation efficiency [5, 6]. Ma et al. proposed in the numerical study that an optimal confinement appears in the indentation process for various confinements, based on various crack propagation degrees [7]. Moreover, rock may fail in a brittle manner or a ductile manner [8, 9] because of the promoted crack propagation in rock with high brittleness; Gong and Zhao indicated that cutting efficiency is affected by the rock brittleness [10].

The aforementioned studies indicated that indentation efficiency is significantly determined by the crack propagation caused by indentations. To promote rock breakages in
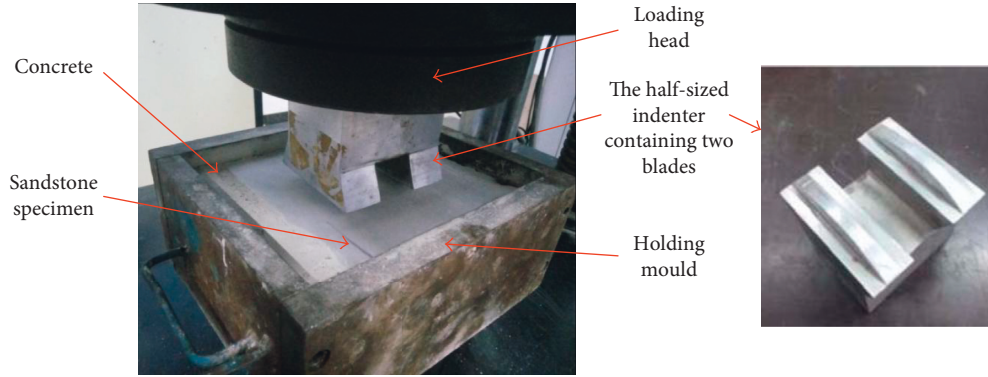
FIGURE 1: Experimental preparation and the indenter.

TABLE 1: Main mechanical parameters of the rock samples.

Mechanical parameters	Density (g/cm^3)	Elastic modulus (GPa)	Poisson's ratio	Uniaixial compression strength (MPa)	Tensile strength (MPa)	Friction angle (°)
Value	2.5	17.1	0.25	29.5	9.2	41.6

target rock, extensive laboratory and numerical studies have been conducted from a machinery point of view. Besides the indenter shape and size, the indentation rate, and the loading sequence, the spacing and penetration (indentation depth) are the main machinery factors that may affect rock breakages and cutting efficiency [11–15]. For instance, an optimal spacing of 76 mm was proposed by Gertsch et al. in a laboratory study where a hard rock was tested [16]. Liu et al. proposed in the laboratory tests that over, moderate, and insufficient breakages sequentially occur with the increase in spacing [17]. Moon and Oh proposed that the optimal spacing-penetration (s/p) ratio is about 10 when the indentation depth is 5 mm [18]. Some other laboratory tests also proposed similar conclusions based on the collected chips and the consumed energy [19–22]. In the aforementioned studies, based on the formed groove volumes or chip weight and the consumed energy, the optimal s/p ratios were comprehensively studied. However, the dynamic crack propagation that may determine the indentation force and the chip formation for various s/p ratios has hardly been investigated.

Thus, in the present article, a series of indentation tests on sandstone specimens, using half-sized indenters with various spacings, was performed to investigate the dynamic indentation characteristics for various s/p ratios. To further study the internal crack propagation for various s/p ratios, a numerical study based on the 2D Particle Flow Code was conducted. The relation between crack stress concentrations and fluctuations of indentation force was investigated. Finally, with the laboratory results, the optimal s/p ratios were also discussed.

2. Laboratory Tests

2.1. Rock Samples and Test Preparation. Figure 1 shows the sandstone specimens with the main mechanical parameters in Table 1. These specimens were cuboids with a length,

TABLE 2: Spacing and indentation depth in laboratory tests.

Spacing (mm)	60	70	80
Indentation depth (mm)	7	7	7
	7.7	7.7	7.7
	8	—	—
	8.3	8.3	8.3
	9	—	—
	—	9.5	9.5
	—	—	10

a width, and a thickness of 25 cm, 25 cm, and 10 cm, respectively. According to previous studies, the size effect is negligible when the ratio of the plastic zone depth to the minimum depth of the sample is lower than 1/6. Based on the equation of the plastic zone depth [5, 6], the plastic zone depth was 1.9 mm, whereas the minimum width of the sample was 100 mm. The aforementioned ratio was much lower than 1/6. Thus, the size effect is negligible in the present article.

According to the previous measures, applied to simulate rock breakages in approximately practical conditions [16, 22], specimens were cast by concrete in a holding mould before indentations (Figure 1). After a curing process for 20 days, the indenters, containing two half-sized TBM blades with three spacings of 60 mm, 70 mm, and 80 mm, were placed under the loading head (Figure 1). In the indentation process, the indenter was displacement-controlled with a relative rate of 0.5 mm/min proposed by Liu et al. [6]. The indentation force was recorded every few seconds by an affiliated computer system. Then, the indentation energy can be obtained by integrating the indentation displacement and the indentation force. The blades were half-sized to ensure the efficient rock breakages between blades; therefore, larger indentation depths than those adopted in previous studies were applied in the present article [6]. The corresponding spacings and indentation depths are listed in Table 2. After
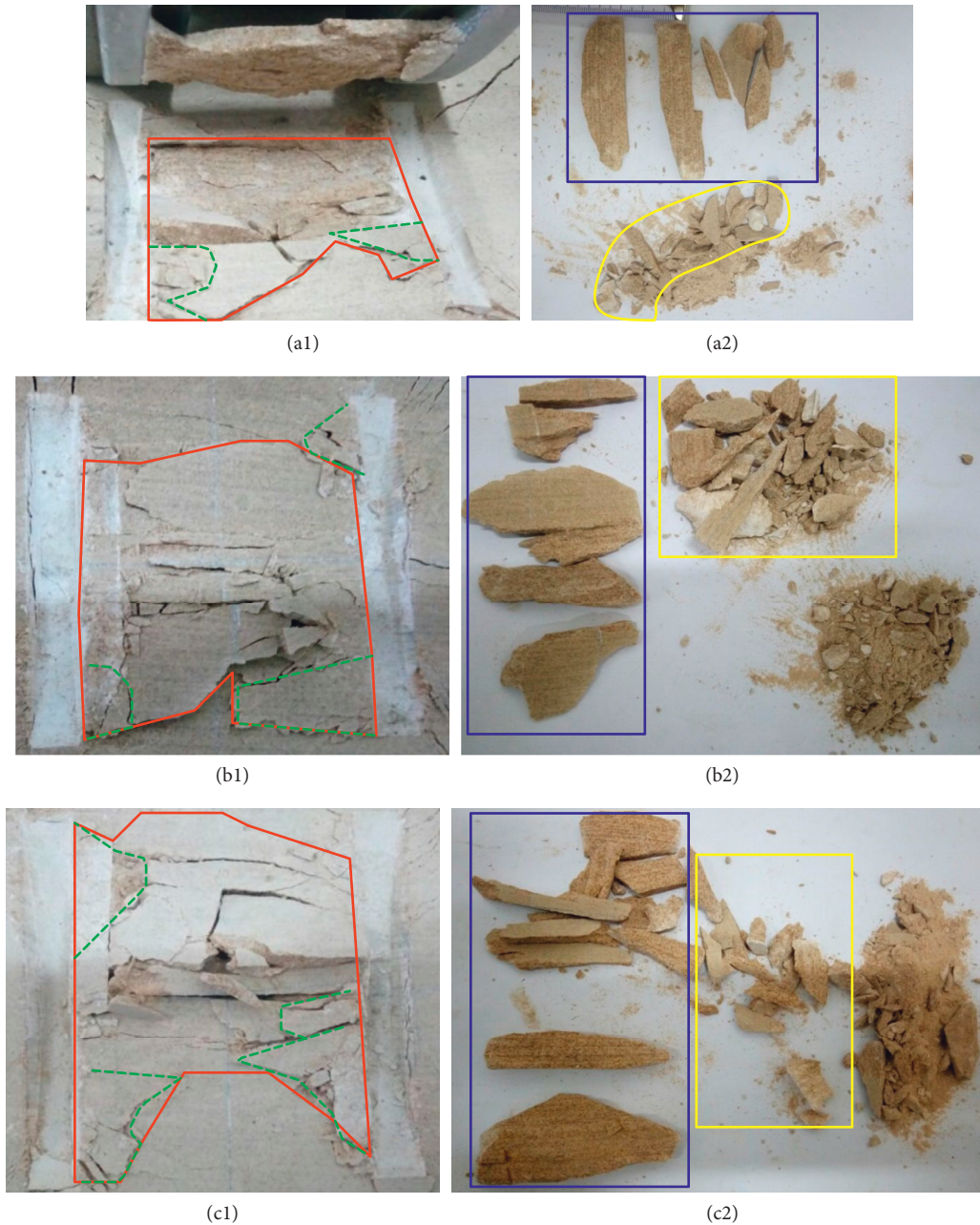
(a1)

(a2)

(b1)

(b2)

(c1)

(c2)

Figure 2: Rock breakages for the spacing of 80 mm when the indentation depths were (a1, a2) 7 mm, (b1, b2) 7.7 mm, and (c1, c2) 8.3 mm.

indentations, the chips and crushed rock powder were collected and weighted. Then, the groove volumes were obtained by dividing the total weight of chips and the powder by the sandstone density.

2.2. Laboratory Results. Groove volumes, influenced by rock breakages, and indentation energy, determined by the indentation force, are two factors, determining the indentation efficiency. Thus, these two factors are mainly discussed in the following sections.

2.3. Rock Breakages in Laboratory Tests. Figure 2 depicts the typical rock breakages when the indentation depths were 7 mm, 7.7 mm, and 8.3 mm for a spacing of 80 mm. The red line in Figure 2(a1) depicts the fractured area when the indentation depth was 7 mm, and the green dash lines indicated that many small chips formed at shallow parts of the indented rock. Therefore, Figure 2(a2) shows some large chips and many small chips enclosed in the blue line and the yellow line, respectively, formed. In addition, rock powders that may result from crushing were collected. When the indentation depth increased to 7.7 mm, the fracture area
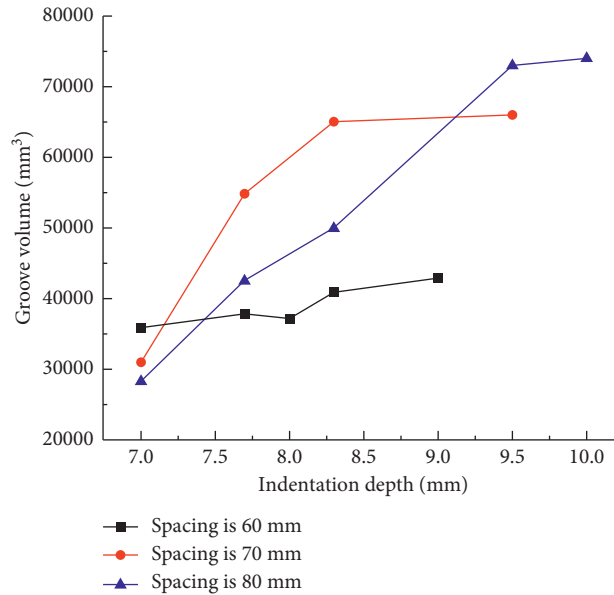
Figure 3: Groove volumes.

denoted by the red line increased between the blades (Figure 2(b1)). Additionally, Figure 2(b2) shows that the chips also consisted of large chips, small chips, and rock powders. However, the proportion of the powder may have increased because of the increased crushing. When the indentation depth further increased to 8.3 mm, the breakage area further increased. This increase further contributed to the formation of the large chips and rock powder. It can be concluded that chips between indentations consist of large chips, small chips form at shallow rock, and rock powder caused by crushing. In addition, with the increase in indentation depth, many large chips form. Simultaneously, more rock powders form by the promoted crushing. Thus, rock breakages are promoted with the increase of the indentation depth, and this inference is affirmed by the curves in Figure 3. It is interesting to note that groove volumes first significantly increased and subsequently slightly increased with the increase in indentation depth when the spacings were 70 mm and 80 mm.

The typical rock breakages for increasing spacings, when the indentation depth was fixed, are depicted in Figure 4. When the spacing was 60 mm, Figure 4(a) shows that fierce rock breakages occurred and formed many irregular small chips. When the spacing increased to 70 mm, the rock breakage degree was restrained. However, effective crack incisions denoted by red lines were observed (Figure 4(b)). When the spacing further increased to 80 mm, rock breakage degree was further restrained with shrunken fracture area and less effective crack incisions. Similar phenomena for increasing spacings were reported by Liu et al. [17].

2.4. Indentation Force and Energy in Laboratory Tests. Indentation energy, obtained by integrating the indentation force and the displacement, is the other critical factor that determines the indentation efficiency. Figure 5 depicts the typical indentation force-depth curve. At the early

indentation stage, a slight increase of the indentation force, resulting from the compaction of the rock beneath the blades, was observed with the increase in indentation depth. With further increase in indentation depth, the increasing tendency of the indentation force was accelerated at the middle indentation stage. The rock under the indenters was highly compacted at the middle indentation stage; thus, the indentation force for a unit increase in indentation depth is increased. When the indentation depth increased to about 5.9 mm, the first peak point of the indentation force, followed by a sudden drop, was observed. After the sudden drop of the indentation force, relatively moderate increases and sudden drops of the indentation forces were observed. In other words, fluctuations of the indentation force occurred. These fluctuations that may relate to the crack propagation were also observed in previous studies [6]. After the integration of the indentation force and the indentation displacement, the consumed energy for various indentation tests is depicted in Figure 6. The fitted curves indicate that indentation energies approximately increased with the increase in indentation depth. Figure 6 also shows that the indentation energy increased with the increase in spacing when the indentation depth was relatively low. The less impair effect on the rock integrity for the longer spacing, exerted by the adjacent indentation, may properly verify this phenomenon.

3. Numerical Tests

The above laboratory tests indicate that rock breakages between indentations consisted of large chips, small chips at shallow parts, and crushed powders. In addition, the indentation force fluctuated with the increase in indentation depth. However, due to the limit on laboratory equipment, the dynamic chip formation process, hardly reported in previous studies, has not been properly studied. In addition, the relation between chip formation and fluctuations of the
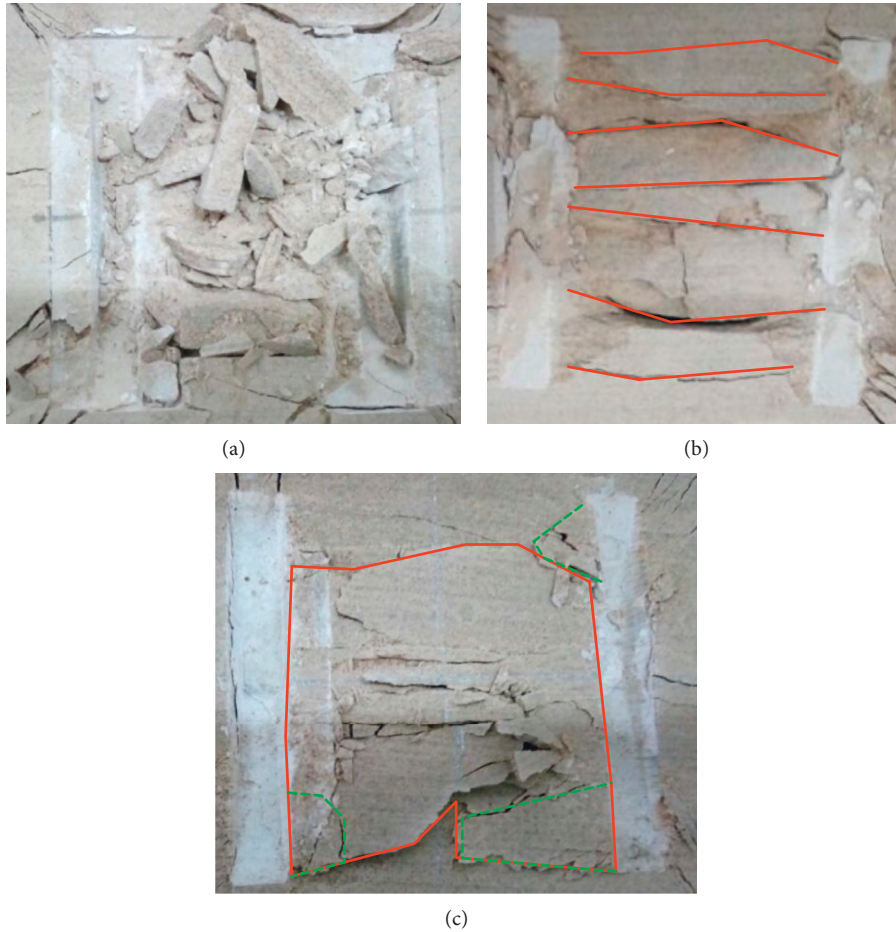
(a)

(b)

(c)

FIGURE 4: Rock breakages for the indentation depth of 7.7 mm when the spacings were (a) 60 mm, (b) 70 mm, and (c) 80 mm.
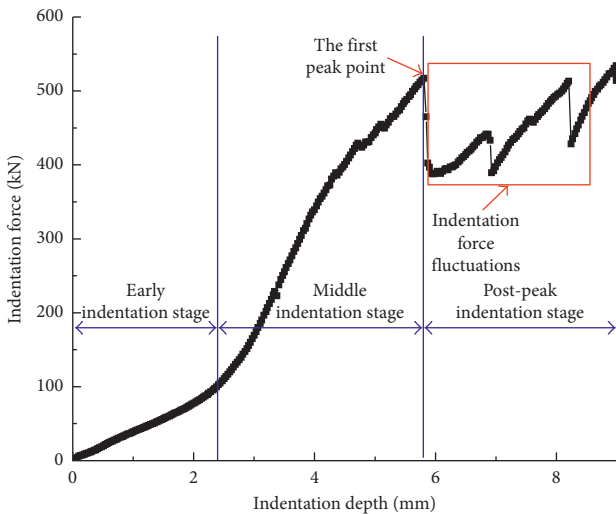

FIGURE 5: The typical indentation force-depth curve.

Spacing is 60 mm
Spacing is 70 mm
Spacing is 80 mm

FIGURE 6: The indentation energies for various indentation tests.

indentation force remains unclear. Moreover, the previous study showed that the practical cutting condition can be simplified into the plane strain condition [7]. Correspondingly, the indentation problem can be reasonably simplified as a 2D plane strain [7]. Thus, a widely used DEM code, PFC 2D, was applied to discuss the above problems.

In the numerical simulations, the rock breakages, caused by crack propagation, and the fluctuations of the indentation forces were discussed.

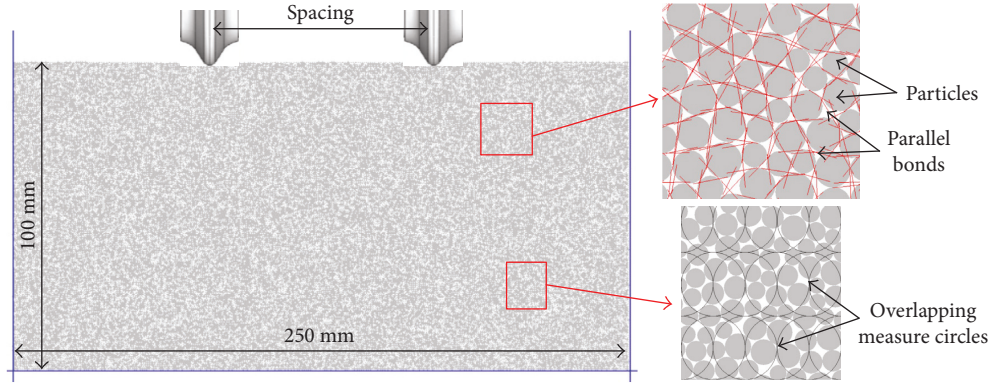FIGURE 7: Numerical model and preparation.

TABLE 3: Micro- and macrosynthetic parameters.

Microparameters	Values	Macroparameters	Value
Minimum radius (mm)	0.3		
R_{max}/R_{min}	1.66	Uniaxial compression stress, UCS (MPa)	28.3
Particle contact modulus (GPa)	9.5		
Particle normal/shear stiffness	2.5		
Friction coefficient	0.5	Young's modulus, E (GPa)	2.2
Parallel bond modulus (GPa)	19.5		
Parallel normal/shear stiffness	2.5		
Parallel bond normal strength (MPa)	16.7	Poisson ratio	0.23
Parallel bond shear strength (MPa)	17.8		

3.1. Numerical Model and Preparation. The length and height of the numerical model, consisting of 48530 particles, were 250 mm and 100 mm, respectively (Figure 7). In an actual rock, shear, tensile, and bending stresses are likely to act on the bonds between particles. Thus, parallel bonds that are capable of resisting shear, tension, and moment were installed between particles. Before indentations, a calibration of the uniaxial compression test was performed according to the previous calibration of rocks [23]. The micro- and macromechanical parameters are listed in Table 3. According to the specifications listed in Table 2, three series of indentation tests for the spacings of 60 mm, 70 mm, and 80 mm were performed. In these simulations, the indenters were also displacement-controlled with a rate of 0.5 mm/min. Previous studies indicated that the concentrated stresses, leading to strain concentrations, are responsible for the crack initiation and propagation in rock specimens [24, 25]. Therefore, to monitor the stress evolution in the indentation process, 10,000 measure circles with a radius of 1 mm were installed in the specimens (Figure 7). To accurately measure the stresses, including the horizontal stress, the vertical stress, and the shear stress, the measure circles overlapped with adjacent ones. We could characterize the tensile crack propagation by tracking the positive maximum principle stress:

$$\sigma_{max} = \frac{\sigma_h + \sigma_v}{2} + \sqrt{\left(\frac{\sigma_h - \sigma_v}{2}\right)^2 + \tau^2}, \qquad (1)$$

where σ_{max} is the maximum principle stress, σ_h and σ_v are the horizontal and vertical stress, and τ is the shear stress.
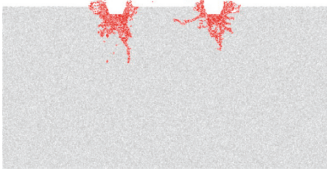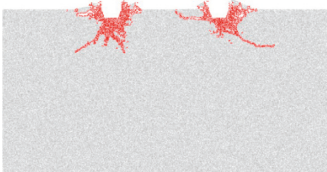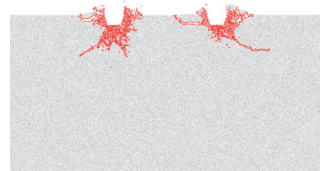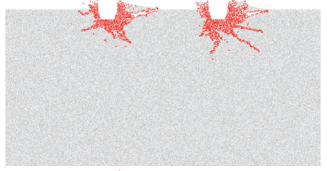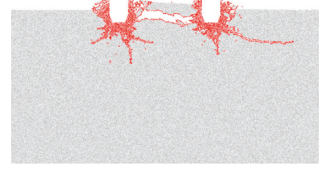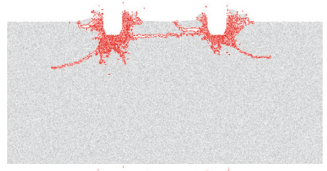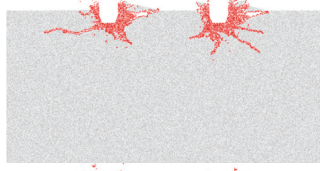
3.2. Numerical Results

3.2.1. Rock Breakages in Numerical Tests. Rock breakages for various spacings and indentation depths are listed in Table 4. The broken particles are drawn in re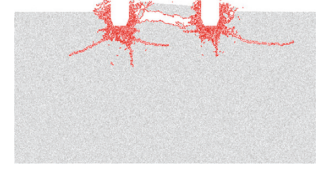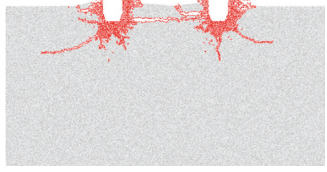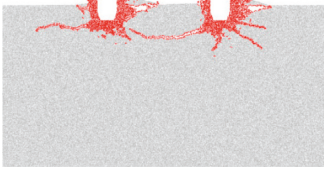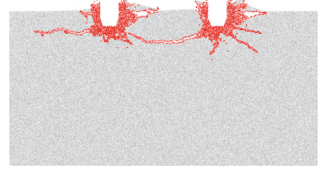d by applying a self-written fish function. When the spacing and indentation depths were 70 mm and 5 mm, small chips formed at shallow surface of the specimen. With further increase in indentation depth to 7 mm, an internal crack connected the adjacent plastic zones; simultaneously, a larger chip was formed by this crack connection. When the indentation depth further increases to 9 mm, internal cracks slightly propagated in the rock; however, the enlarged plastic zones filled with crushed particles, instead of the crack coalescence causing chips, were observed. Similar phenomena are observed for spacings of 60 mm and 80 mm when the indentation depth increases.

The above numerical results agree well with the laboratory tests that rock breakages consisted of large chips, small chips, and rock powders, and it can be further concluded that small chips form first, and then large chips form by crack coalescence with the increase in indentation depth. With further increase in indentation depth, the enlargement of the plastic zones, resulting in more rock powders in laboratory tests instead of the effective crack coalescence, may occur.

Rock breakage areas for various spacings and indentation depths are drawn in Figure 8. For the spacings of 70 mm and 80 mm, small increases of the breakage areas that may result from the continuous expansion of the crushed zones were observed when the indentation depths were

TABLE 4: Rock breakages for various spacings and indentation depths.

	Spacing is 60 mm	Spacing is 70 mm	Spacing is 80 mm
Indentation depth is 5 mm			—
Indentation depth is 6 mm			
Indentation depth is 8 mm			
Indentation depth is 9 mm			
Indentation depth is 10 mm	—	—	

relatively low. Then, because of the formation of the large chips by crack connections, the rock breakage areas significantly increased when the indentation depth increased. With further increases in indentation depth, smaller increases of the breakage area, resulting from the enlargements of the crushed zones, were observed. A similar small increase of the breakage area for the spacing of 60 mm when the depth was higher than 6 mm was observed. Thus, it can be concluded that effective breakage occurs when a critical indentation depth is reached, and then the further increase in indentation depth may fail to increase the chipping.

3.2.2. Indentation Force and Energy. Indentation force curves in Figure 9 indicate that the averaged indentation force rapidly increased at the early indentation stage. The tightly compacted numerical specimen, containing few pores for the further compaction at the early indentation stage, may be responsible for the slight difference from the slightly increased indentation force in laboratory tests. This rapid increase of the indentation force was also observed in the previous numerical study [26]. When the indentation depth reached 0.8 mm, the first peak point of the indentation
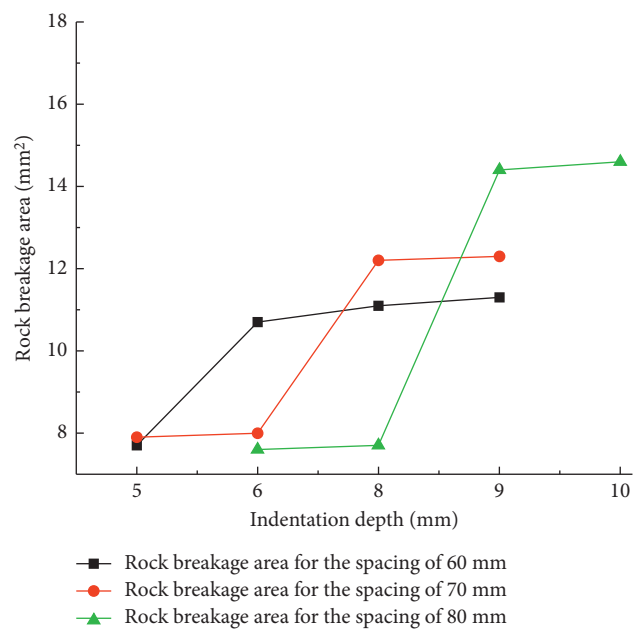

FIGURE 8: Measured rock breakage areas for various spacings and indentation depths.
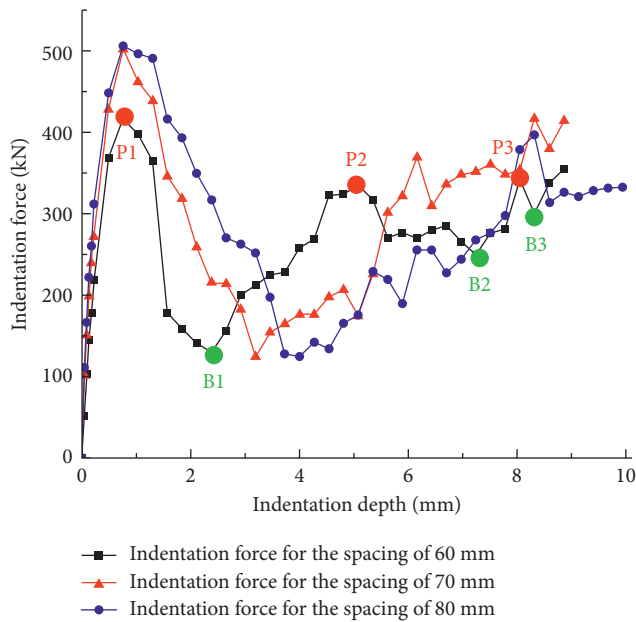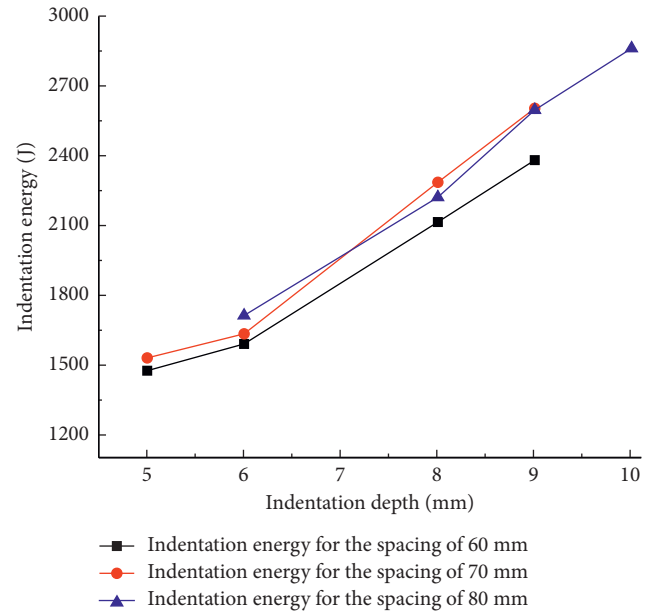
FIGURE 9: Typical indentation force.

FIGURE 10: Numerical indentation energy.

force, P1, was observed on the indentation force curve for the spacing of 60 mm. Then, with further increase in indentation depth, three bottom points, which were B1, B2, and B3 and two peak points, which were P2 and P3, were observed for the indentation depths of 2.4 mm, 5.1 mm, 7.2 mm, 8.1 mm, and 8.3 mm, respectively. Similar tendencies of the indentation force were observed for the other spacings. Thus, the above descriptions show that the characteristics of indentation force agree well with laboratory tests.

The accumulated indentation energy for various spacings and indentation depths shows that indentation energy was approximately linear to the indentation depth (Figure 10), and similar results were obverted in laboratory tests.

4. Discussions

4.1. Relation between Chip Formation and Indentation Force Characteristics. In the above descriptions, similar chipping characteristics and fluctuations of indentation forces were observed in both numerical and laboratory tests. However, the relation between the chip formation and force fluctuations remains unclear.

Therefore, to further investigate the relation between indentation force and crack propagation, the crack propagation conditions at these peak and bottom points for the spacing of 60 mm are shown in Figure 11 where tensile and shear microcracks are depicted in black and red, respectively. Two plastic zones with slightly developed cracks that may result from the increasing indentation force in Figure 9 formed beneath indenters when the indentation depth reached 0.8 mm. When the indentation depth increased to 2.4 mm, cracks enclosed by red ellipses in Figure 11(b) indicate that cracks significantly propagated in the decrease process of indentation force (Figure 9). Then, when the indentation depth further increased to 5.1 mm, the indentation force significantly increased. However, limited crack

propagation in Figure 11(c) was observed. With the further increase in indentation depth to 7.2 mm, the decrease of indentation force in Figure 9 was accompanied with significant crack propagation in Figure 11(d). With the crack propagation in Figures 11(e) and 11(f), and the fluctuations of the indentation force in Figure 9, it can be concluded that crack propagation is accompanied with the decrease of indentation force, whereas the increase of indentation force hardly causes crack propagation.

The stress evolution in the indentation process in Figure 12 may relate to the above force fluctuations and crack propagation. At the early indentation stage, shear stress concentrations formed beneath the indenters, and simultaneously, the tensile stress concentration with the maximum tensile stress of 4.5 MPa located at the rim of the plastic zone and overlapped with the tips of the short cracks (Figure 12(a)). Then, when the tensile or/and shear stress reached the bearing capacity (the shear or tensile strength) of the bonds, cracks initiated and propagated. In the propagation process, both shear and tensile stress concentrations diminished in Figure 12(b). Simultaneously, small chips, enclosed in the green rectangle in Figure 11(b), formed. With the stress concentrations (Figure 12(a)), it can be inferred that these small chips may form by both shear failure and tensile failure. The magnified area in Figure 11, where the black and the red microcrack represent the tensile and the shear failure, verifies that these chips formed by both shear and tensile stress concentrations. However, due to the relatively large distance between adjacent plastic zones, the internal crack, also initiating from the shear and tensile overlapping zones, failed to connect these plastic zones. Simultaneously, the crack propagation significantly impaired the firm contacts between the indenters and the particles; therefore, the indentation force dramatically decreased. In addition, the overlaps of the tensile concentration zones and the crack tips indicate that the positive maximum principle stress can successfully track the crack propagation.
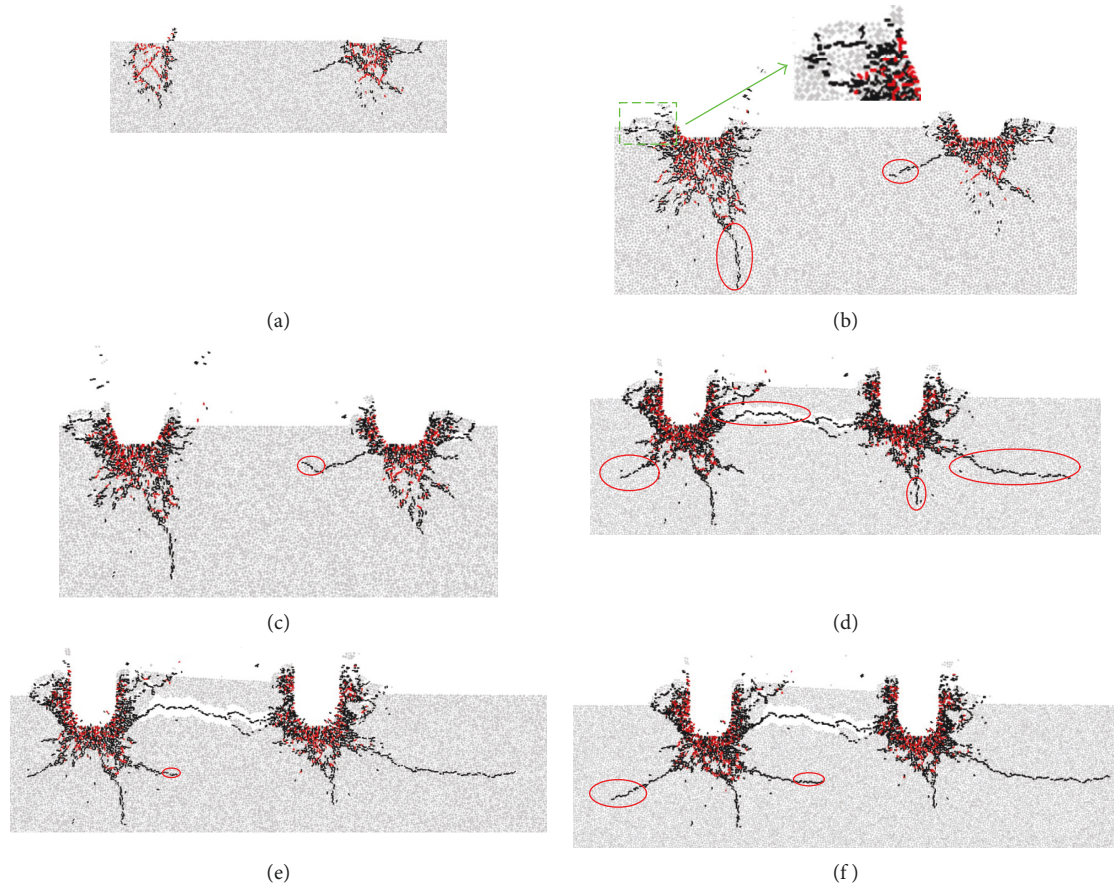
FIGURE 11: Crack propagation at peak and bottom points: (a), (b), (c), (d), (e), and (f) are the crack propagation conditions at P1, B1, P2, B2, P3, and B3.
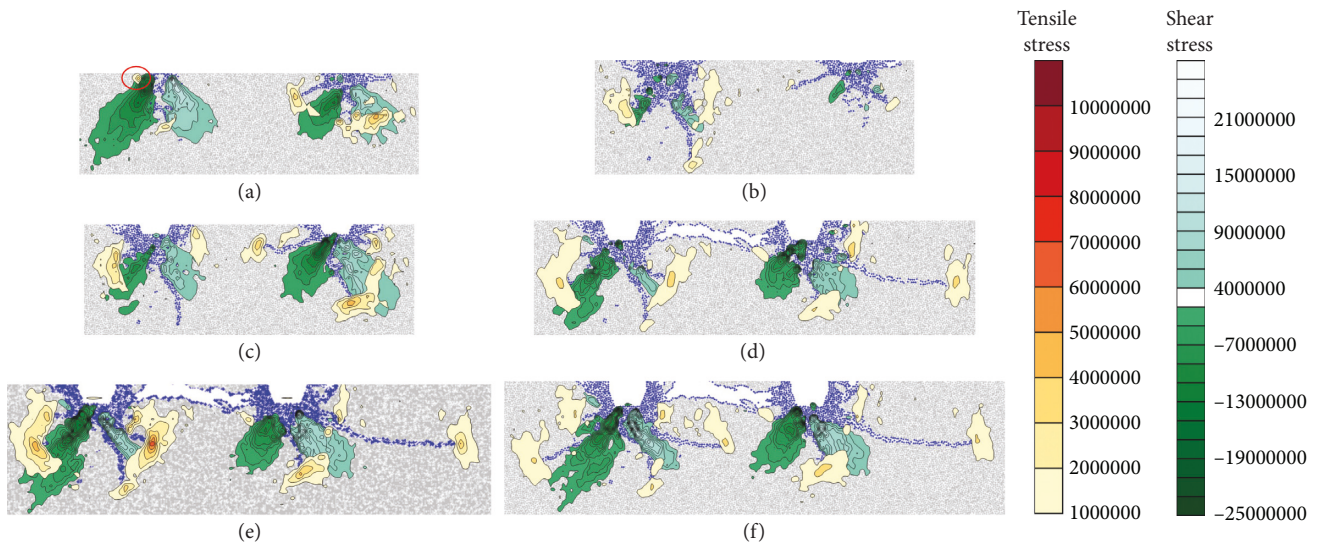

FIGURE 12: Stress distributions at peak and bottom points: (a), (b), (c), (d), (e), and (f) are the stress distributions at P1, B1, P2, B2, P3, and B3.

With further increase of indentation depth to 5.1 mm, crack propagation ceased, thus, the contacts between the indenters and the particles were strengthened, leading to the increase in indentation force. Simultaneously, the shear and tensile stress concentrations developed because of the increase in indentation force and the cessation of the crack propagation. Therefore, obvious tensile concentration zones with the maximum tensile stress of 4.8 MPa formed at the
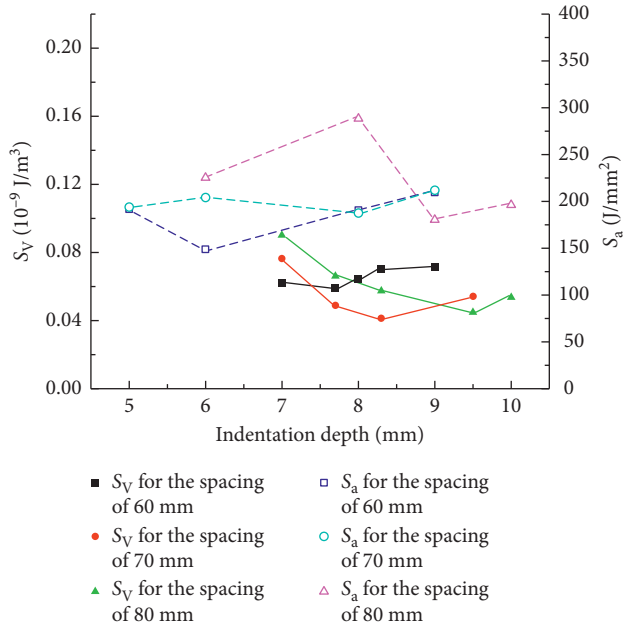
FIGURE 13: Indentation efficiency in numerical and laboratory tests.

crack tips (Figure 12(c)). When the tensile and/or shear stress reached the bearing capacity again, similar cracks propagation, leading to the large chip formation in deeper rock and accompanied by the drop of the indentation force and dissipation of stress concentrations, occurred (Figures 9 and 12(d)). Similar phenomena of crack propagation, indentation force variation, and stress evolution were observed with further increase in indentation depth.

Thus, it can be concluded that shear and tensile stress concentrations are responsible for both small and large chip formations. Usually, crack propagation leads to the sharp force drop and the stress dissipations at crack tips. Then, crack propagation ceases when the concentrated stress is not high enough for crack propagation. The cessation of the crack propagation leads to the rock compaction beneath the indenters with further increase of indentation depth. In the compaction process, the indentation force increases and promotes the stress concentrations around the plastic zones and the crack tip. When the stress concentrations increase to a certain degree, cracks propagate. Another cycle, characterized by crack propagation and cessation, indentation force fluctuations and stress concentrations and dissipations will be observed with further increase of indentation depth. In addition, small chips form at shallow parts at the early indentation stage, then, the accumulation of the internal cracks forms the large chip. With further increase in indentation depth, the internal crack propagation may fail to form additional chips. This conclusion may verify why the groove volume slightly increases with the increase in indentation depth that is higher than some values (Figures 3 and 8).

4.2. Indentation Efficiency. The specific energy is an efficient indicator, charactering indentation efficiency. In the present

article, because the numerical study was conducted in a plane condition, the specific energy can be expressed in two forms [17]:

$$
\begin{aligned}
S_V &= \frac{W}{V}, \\
S_a &= \frac{W}{A},
\end{aligned}
\tag{2}
$$

where S_V and S_a are the specific energy for laboratory and numerical studies, respectively, W is the indentation energy, V is the groove volumes in laboratory tests, and A is the breakage area in numerical tests.

The calculated specific energy for various spacings and indentation depths are drawn in Figure 13. The laboratory results indicate that the specific energy first decreased with the increase in indentation depth. These decreases denote that indentation efficiency was promoted by the increased indentation depth. However, the specific energy subsequently increased with the further increase in indentation depth when the depth was higher than a critical value. The decrease and increase of the specific energy with the increase in indentation depth indicate that an optimal indentation depth for the specific spacing existed. When the spacing increased from 60 mm to 80 mm, the optimal indentation depth increased from about 7.7 mm to 9.5 mm. Thus, the optimal spacing-to-indentation (s/p) ratio ranges from 7.8 to 8.4 in the laboratory tests. With the optimal s/p ratios reported in previous studies [14–16], the smaller optimal s/p ratios in the present article may result from the shrunken indenter size.

In numerical studies, a similar tendency of the specific energy was observed when the spacing was 60 mm. The optimal s/p ratio was about 10. When the spacing increased to 70 mm and 80 mm, an increase in the specific energy occurred before the decrease. These increases may result from the limited chipping area of the small chips, and the increased indentation energy before large chip formation. When the indentation depth further increased, the large chip formation led to the decrease of the specific energy (Table 4). Then, the continuous indentation, consuming much indentation energy and generating few chips, resulted in the increase of the specific energy. Similarly, for various spacings in numerical studies, the optimal s/p ratio, ranging from 8.8 to 10, was also slightly lower than those reported. The shrunken indenter size may be responsible for these lower ratios.

It can be concluded from above analysis that the increased spacing results in the increase of the optimal indentation depth. The effective crack connections between indentations are responsible for the increased indentation efficiency.

5. Conclusions

To investigate the dynamic indentation characteristics for various spacings and indentation depths, laboratory and numerical indentation tests were conducted. The results indicate that small chips formed at the early indentation

stage. Then, large chips, resulted from crack coalescence, formed when the indentation depth was large enough. With further increase in indentation depth, few chips formed. Therefore, an optimal indentation depth existed for the specific spacing. However, the s/p ratio ranged in a limited scope. In addition, the crack propagation that weakened the contact between the indenter and the specimen resulted in the stress dissipations at crack tips and the drop of the indentation force, whereas the cessation of the crack propagation led to the stress concentration with the increase in indentation depth.

Conflicts of Interest

The authors declare that they have no conflicts of interest.

Acknowledgments

References

[1] Y. L. Zhao, L. Y. Zhan, W. J. Wang, J. Z. Tang, H. Lin, and W. Wan, "Transient pulse test and morphological analysis of single rock fractures," *International Journal of Rock Mechanics and Mining Sciences*, vol. 91, pp. 139–154, 2017.

[2] J. Liu, P. Cao, Z. Jiang, Y. L. Zhao, and R. H. Cao, "Numerical simulation on effects of embedded crack on rock fragmentation by a tunnel boring machine cutter," *Journal of Central South University*, vol. 21, no. 8, pp. 3302–3308, 2014.

[3] X. Fan, R. Chen, H. Lin, H. P. Lai, C. Y. Zhang, and Q. H. Zhao, "Cracking and failure in rock specimen containing combined flaw and hole under uniaxial compression," *Advances in Civil Engineering*, vol. 2018, Article ID 9818250, 15 pages, 2018.

[4] Q. M. Gong, J. Zhao, and Y. Y. Jiao, "Numerical modeling of the effects of joint orientation on rock fragmentation by TBM cutters," *Tunneling and Underground Space technology*, vol. 20, no. 2, pp. 183–191, 2005.

[5] L. J. Yin, Q. M. Gong, H. S. Ma, J. Zhao, and X. B. Zhao, "Use of indentation tests to study the influence of confining stress on rock fragmentation by a TBM cutter," *International Journal of Rock Mechanics and Mining Sciences*, vol. 72, pp. 261–276, 2014.

[6] J. Liu, P. Cao, and D. Y. Han, "Sequential indentation tests to investigate the influence of confining stress on rock breakage by tunnel boring machine cutter in a biaxial state," *Rock Mechanics and Rock Engineering*, vol. 49, no. 4, pp. 1479–1495, 2016.

[7] H. S. Ma, L. J. Yin, and H. G. Ji, "Numerical study of the effect of confining stress on rock fragmentation by TBM cutter," *International Journal of Rock Mechanics and Mining Sciences*, vol. 48, no. 6, pp. 1021–1033, 2011.

[8] Y. L. Zhao, Y. X. Wang, W. J. Wang, W. Wan, and J. Z. Tang, "Modeling of non-linear rheological behavior of hard rock using triaxial rheological experiment," *International Journal of Rock Mechanics and Mining Sciences*, vol. 93, pp. 66–75, 2017.

[9] Y. L. Zhao, L. Y. Zhang, W. J. Wang, W. Wan, and W. H. Ma, "Separation of elasto-visco-plastic strains of rock and a non-linear creep model," *International Journal of Geomechanics*, vol. 18, no. 1, 2018.

[10] Q. M. Gong and J. Zhao, "Influence of rock brittleness on TBM penetration rate in Singapore granite," *Tunnelling and Underground Space Technology*, vol. 22, no. 3, pp. 317–324, 2007.

[11] H. Haeri, M. F. Marji, and K. Shahriar, "Simulating the effect of disc erosion in TBM disc cutters by a semi-infinite DDM," *Arabian Journal of Geosciences*, vol. 8, no. 6, pp. 3915–3927, 2014.

[12] Z. X. Zhang, "Estimate of loading rate for a TBM machine based on measured cutter forces," *Rock Mechanics and Rock Engineering*, vol. 37, no. 3, pp. 239–248, 2004.

[13] Q. Tan, Z. J. Xu, Y. M. Xia, and K. Zhang, "Numerical study on mode of breaking rock by TBM cutter in two cutting orders," *Journal of Central South University*, vol. 43, no. 3, pp. 940–949, 2012, in Chinese.

[14] J. W. Cho, S. Jeon, S. H. Yu, and S. H. Chang, "Optimum spacing of TBM disc cutters: a numerical simulation using the three-dimensional dynamic fracturing method," *Tunnelling and Underground Space Technology*, vol. 25, no. 3, pp. 230–244, 2010.

[15] S. Choi and S. Lee, "Three-dimensional numerical analysis of the rock-cutting behavior of a disc cutter using particle flow code," *KSCE Journal of Civil Engineering*, vol. 19, no. 4, pp. 1129–1138, 2015.

[16] R. Gertsch, L. Gertsch, and J. Rostami, "Disc cutting tests in colorado red granite: implications for TBM performance prediction," *International Journal of Rock Mechanics and Mining Sciences*, vol. 44, no. 2, pp. 238–246, 2007.

[17] J. Liu, P. Cao, and D. Y. Han, "The influence of confining stress on optimum spacing of TBM cutters for cutting granite," *International Journal of Rock Mechanics and Mining Sciences*, vol. 88, pp. 165–174, 2016.

[18] T. Moon and J. Oh, "A study of optimal rock-cutting conditions for hard rock TBM using the discrete element method," *Rock Mechanics and Rock Engineering*, vol. 45, pp. 837–849, 2012.

[19] H. Haeri and M. F. Marji, "Simulating the crack propagation and cracks coalescence underneath TBM disc cutters," *Arabian Journal of Geosciences*, vol. 9, no. 2, 2016.

[20] C. Labra, J. Rojek, and E. Oñate, "Discrete/finite element modelling of rock cutting with a TBM disc cutter," *Rock Mechanics and Rock Engineering*, vol. 50, no. 3, pp. 621–638, 2016.

[21] H. S. Ma, Q. M. Gong, J. Wang, L. Yin, and X. Zhao, "Study on the influence of confining stress on TBM performance in granite rock by linear cutting test," *Tunnelling and Underground Space Technology*, vol. 57, pp. 145–150, 2016.

[22] J. W. Cho, S. Jeon, H. Y. Jeong, and S. H. Chang, "Evaluation of cutting efficiency during TBM disc cutter excavation within a Korean granitic rock using linear-cutting-machine testing and photogrammetric measurement," *Tunnelling and Underground Space Technology*, vol. 35, pp. 37–54, 2013.

[23] R. H. Cao, P. Cao, X. Fan, X. Xiong, and H. Lin, "An experimental and numerical study on mechanical behavior of ubiquitous-joint brittle rock-like specimens under uniaxial

compression," *Rock Mechanics and Rock Engineering*, vol. 49, no. 11, pp. 4319–4338, 2016.

[24] Y. L. Zhao, L. Y. Zhang, W. J. Wang, C. Z. Pu, W. Wan, and J. Z. Tang, "Cracking and stress–strain behavior of rock-like material containing two flaws under uniaxial compression," *Rock Mechanics and Rock Engineering*, vol. 49, no. 7, pp. 2665–2687, 2016.

[25] H. Lin, W. Xiong, and Q. Yan, "Three dimensional effect of tensile strength in the standard Brazilian test considering contact length," *Geotechnical Testing Journal*, vol. 39, no. 1, pp. 137–143, 2015.

[26] X. Zhu, W. Liu, and X. He, "The investigation of rock indentation simulation based on discrete element method," *KSCE Journal of Civil Engineering*, vol. 21, no. 4, pp. 1201–1212, 2016.